In situ Mössbauer spectroscopy study of the activation and reducibility of chromium- and aluminium-doped iron oxide based water-gas shift catalysts under industrially relevant conditions

Ariëns, M. I.; Brück, E.; van de Water, L. G.A.; Hensen, E. J.M.; Dugulan, A. I.

DOI
10.1016/j.apcatb.2024.124316

Publication date
2024

Document Version
Final published version

Published in
Applied Catalysis B: Environmental

Applied Catalysis B: Environment and Energy 357 (2024) 124316

Contents lists available at ScienceDirect

Applied Catalysis B: Environment and Energy

journal homepage: www.elsevier.com/locate/apcatb

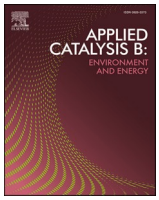

In situ Mössbauer spectroscopy study of the activation and reducibility of chromium- and aluminium-doped iron oxide based water-gas shift catalysts under industrially relevant conditions

M.I. Ariëns [a,b], E. Brück [a], L.G.A. van de Water [c], E.J.M. Hensen [b], A.I. Dugulan [a,*]

[a] Fundamental Aspects of Materials and Energy, Delft University of Technology, Mekelweg 15, Delft, JB 2629, The Netherlands
[b] Laboratory of Inorganic Materials and Catalysis, Department of Chemical Engineering and Chemistry, Eindhoven University of Technology, P.O. Box 513, Eindhoven, MB 5600, The Netherlands
[c] Johnson Matthey, PO Box 1, Belasis Avenue, Billingham, Cleveland TS23 1LB, United Kingdom

ARTICLE INFO

Keywords:
In situ Mössbauer spectroscopy
Water-gas shift
Industrially relevant conditions
Activation
Reducibility

ABSTRACT

The influence of chromium and aluminium doping on the over-reduction during activation of iron-oxide-based water-gas shift catalysts was investigated using Mössbauer spectroscopy for the first time. *In situ* Mössbauer spectra of catalysts exposed to industrially relevant gas compositions were recorded with increasingly reducing *R* factors $R = [CO]*[H_2]/[CO_2]*[H_2O]$. Whereas α-Fe and cementite formed during exposure of a non-doped iron-oxide catalyst to process conditions with an *R* factor of 2.09, such phases were only observed at $R = 4.60$ for a chromium-doped catalyst, showing that chromium stabilizes the catalyst. Over-reduction was enhanced to $R = 2.88$ in a chromium-copper co-doped catalyst. α-Fe was already observed at $R = 1.64$ in an aluminium-doped catalyst, while cementite formation occurred at $R = 2.09$, showing that over-reduction was enhanced, the presence of aluminium delaying carburization. Co-doping copper in the aluminium-doped catalyst showed cementite formation at $R = 2.09$, the same as a non-doped catalyst.

1. Introduction

The water-gas shift (WGS) reaction (1) is industrially employed to increase hydrogen production from natural gas after steam methane reforming (SMR) [1–3]. High CO conversion is achieved by separating the exothermic reaction into two processes [1]. Most CO is removed during the high-temperature (water-gas) shift (HTS) reaction over a copper/chromium doped iron-oxide catalyst between 360 and 450 °C. The concentration of CO in the effluent (2–4 %) is then lowered to ~0.1 % in a low temperature (water-gas) shift (LTS) step over a copper-based catalyst between 190 and 250 °C [1,4].

$$CO + H_2O \rightleftarrows CO_2 + H_2 \quad (1)$$

The active industrial HTS catalyst consists of magnetite (Fe_3O_4) and is formed by exposing a Fe^{3+}-oxide or -oxyhydroxide precursor to WGS conditions [5–7]. Chromium and copper are added to this catalyst as promoters. Chromium exists as Cr^{6+} and Cr^{3+} in the calcined precursor and is incorporated into the magnetite structure during activation, which will reduce Cr^{6+} to Cr^{3+} [7]. The presence of chromium prevents thermal sintering of the active phase and limits the over-reduction of the active magnetite phase to α-Fe and FeC_x [1,4–6,8]. The formation of α-Fe and FeC_x is undesired because such phases catalyse unwanted methanation and Fischer-Tropsch side reactions [9]. Over-reduction is also associated with catalyst pellet degradation, which can induce a significant pressure drop in industrial reactors [9]. Copper is added to commercial catalysts to enhance CO conversion via a chemical promotion mechanism [6,8]. The Wachs group recently showed that divalent copper in the calcined catalyst precursor is removed from the Fe-Cr structure during activation, resulting in Cu^0 nanoparticles partially covered by an iron oxide overlayer on the active chromium-doped magnetite catalyst [8,10]. This results in active sites that are more active than the separate iron oxide and metallic copper sites [11].

The presence of hexavalent chromium, a health concern, in the fresh catalyst has inspired researchers to investigate alternative dopants [2,12–16]. Several groups have shown that aluminium doping resulted in high activity at atmospheric pressure after relatively short reaction times [13,17,18]. We recently demonstrated that industrially relevant chromium/copper- and aluminium/copper-doped catalysts have similar

* Corresponding author.
E-mail address: a.i.dugulan@tudelft.nl (A.I. Dugulan).

https://doi.org/10.1016/j.apcatb.2024.124316
Received 19 March 2024; Received in revised form 10 June 2024; Accepted 17 June 2024
Available online 18 June 2024

Table 1
Phase identification of calcined catalysts (data taken from [19]).

Sample	XRD	Mössbauer spectroscopy at room temperature	Spectral contribution (%)	Mössbauer spectroscopy at −269 °C	Spectral contribution (%)
HM	α-Fe_2O_3	α-Fe_2O_3	100	α-Fe_2O_3	100
Cr-HM	α-Fe_2O_3	α-Fe_2O_3	100	α-Fe_2O_3	100
CrCu-HM	α-Fe_2O_3	Fe^{3+} SPM	100	α-Fe_2O_3	14
				Fe_5HO_8 • 4 H_2O	86
Al-HM	α-Fe_2O_3	Fe^{3+} SPM	100	α-Fe_2O_3	17
				Fe_5HO_8 • 4 H_2O	83
AlCu-HM	*	Fe^{3+} SPM	100	α-Fe_2O_3	5
				Fe_5HO_8 • 4 H_2O	95

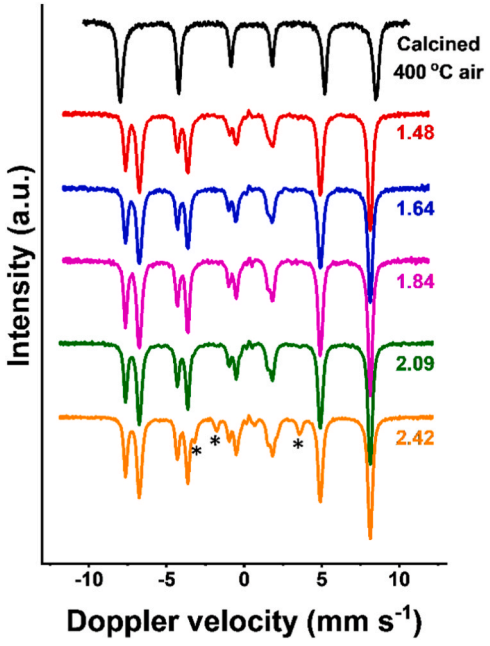

Fig. 1. *In situ* Mössbauer spectra of HM catalyst as a function of H_2O content. Two sextets of magnetite dominate the spectra. Peaks of the cementite sextet are indicated with an (*).

CO conversion at 25 bar after 4 days on stream under industrial HTS conditions [19].

Despite the consensus that aluminium doping results in enhanced thermal stability of the catalyst, no such agreement exists on the influence of aluminium on the reducibility of the fresh and activated catalyst. Meshkani and Rezaei [18] and Araújo and Rangel [20] showed by H_2-TPR that the $Fe_2O_3 \rightarrow Fe_3O_4$ transition is shifted to lower temperatures in the presence of aluminium. Thus, aluminium can enhance the reducibility of the Fe_2O_3. Nevertheless, these authors did not observe an influence of aluminium doping on the $Fe_3O_4 \rightarrow$ FeO and FeO → α-Fe transitions. Jeong et al. [21] followed a similar effect of aluminium doping. In their catalysts, the $Fe_2O_3 \rightarrow Fe_3O_4$ transition shifted to lower temperatures, while the over-reduction peak of Fe_3O_4 was not distinct enough to interpret. In contrast, Natesakhawat et al. [17] showed that aluminium doping did not affect the $Fe_2O_3 \rightarrow Fe_3O_4$ transition, while the $Fe_3O_4 \rightarrow$ FeO, α-Fe transition shifted to higher temperatures. Comparing such TPR results is likely complicated by using different heating rates, catalyst preparation methods, and phases in the catalyst precursors. We recently showed in two separate studies that the calcined catalyst precursor could contain a significant amount of small amorphous ferrihydrite (Fe_5HO_8 • 4 H_2O) particles, partially invisible to XRD analysis, in addition to hematite (α-Fe_2O_3), typically observed as the dominant phase by XRD [6,19]. The presence of ferrihydrite unequivocally demonstrated by ^{57}Fe Mössbauer spectroscopy complicates the interpretation of the TPR patterns because of overlapping reduction features with hematite [22]. In H_2-TPR, over-reduction of magnetite leads to reduction features between 650 °C and 770 °C [17,18,21], which is far above realistic industrial HTS conditions (typically in the range of 360–450 °C). However, over-reduction during the WGS reaction also depends on the concentration of reducing and oxidising gasses [2]. When studying aluminium-doped iron oxides, the precipitation rate of iron and aluminium species relies heavily on the pH. Natesakhawat et al. [17] suggested that low pH favours iron precipitation, while high pH favours aluminium precipitation. They showed that a catalyst prepared at pH = 9 provided the highest CO conversion in the pH = 8–11 preparation range. The authors proposed that precipitated aluminium species start to dissolve at pH > 9, possibly due to the amphoteric nature of aluminium. This suggests that not all aluminium added for precipitation is incorporated into the catalyst structure when catalysts are aged at elevated pH and possibly a separate alumina phase is formed. While alumina itself is not reducible, an impact on H_2-TPR data can be expected because aluminium can enter the iron oxide phases. This can explain the different outcomes of TPR measurements reported for aluminium-doped iron oxides.

Table 2
Fitting parameters of *in situ* Mössbauer spectra HM catalyst.

R	Phase	IS (mm s^{-1})	QS (mm s^{-1})	Hyperfine field (T)	Linewidth (mm s^{-1})	Spectral contribution (%)
1.48	Fe_3O_4(tet)	0.27	-0.01	49.1	0.29	35
	Fe_3O_4(oct)	0.67	0.01	45.8	0.26	65
1.64	Fe_3O_4(tet)	0.27	-0.01	49.1	0.28	35
	Fe_3O_4(oct)	0.67	0.02	45.9	0.25	65
1.84	Fe_3O_4(tet)	0.27	-0.01	49.1	0.26	36
	Fe_3O_4(oct)	0.67	0.01	45.9	0.23	64
2.09	Fe_3O_4(tet)	0.27	0.00	49.1	0.27	35
	Fe_3O_4(oct)	0.67	0.01	45.8	0.24	62
	α-Fe	0.00	0.00	32.1	0.5	1
	Fe_3C	0.18	0.00	21.0	0.5	2
2.42	Fe_3O_4(tet)	0.27	0.00	49.1	0.27	32
	Fe_3O_4(oct)	0.67	0.01	45.9	0.25	56
	Fe_3C	0.18	0.02	21.0	0.34	12

Experimental uncertainties: Isomer shift: IS ± 0.01 mm^{-1}, quadrupole splitting: QS ± 0.01 mm s^{-1}, line width: Γ ± 0.01 mm^{-1}, hyperfine magnetic field: ± 0.1 T, spectral contribution: ± 3 %.

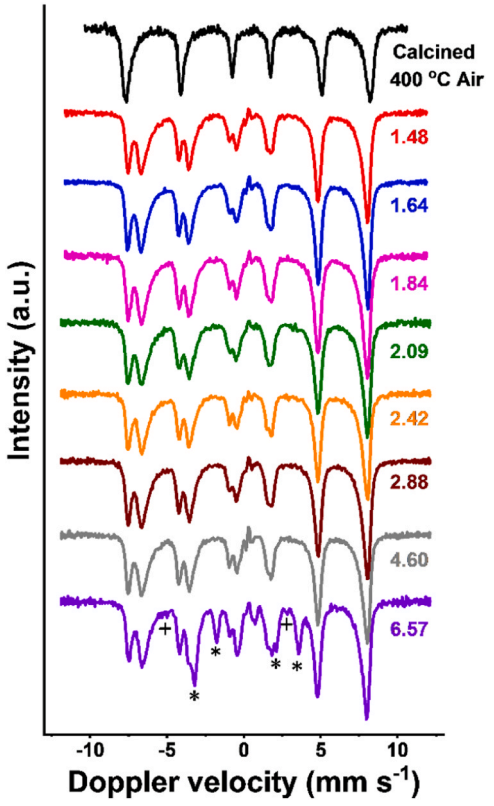

Fig. 2. *In situ* Mössbauer spectra of Cr-HM catalyst compared to *ex situ* spectrum of calcined catalyst. Visible peaks of the cementite sextet are indicated with an asterisk (*), those of α-Fe with a plus (+).

Herein we investigated, with XRD and Mössbauer spectroscopy, two well-known bulk representative methods, the stability of aluminium- and chromium-doped magnetite with and without copper promoter under industrially relevant reaction conditions. The effect of dopants on FeO, α-Fe, and FeCx formation was investigated with *in situ* Mössbauer spectroscopy. Mössbauer spectroscopy has been used extensively to study the formation of FeC_x phases in iron-based Fischer-Tropsch catalysts because of its high sensitivity for bulk iron species [23,24]. In the present work, we exposed model HTS catalysts to increasingly reducing gas atmospheres by decreasing the steam partial pressure in a simulated HTS gas mixture containing H_2, CO, CO_2, He, and H_2O.

2. Experimental

2.1. Catalyst preparation

Catalysts were prepared via a single-step co-precipitation/calcination route [5,6,19]. In brief, appropriate amounts of iron, chromium, aluminium, and copper nitrates were dissolved in deionised water at 60 °C. The metals were precipitated by adding a NaOH solution until the pH reached 10. The resulting slurry was aged for 1 hour at 60 °C, after which the precipitates were washed with hot (60 °C) deionised water. After washing, the precipitates were dried at 150 °C for 3 hours and calcined at 400 °C for 4 hours in static air. Typical chromium and copper contents of commercial HTS catalysts are 8 wt% and 3 wt%, respectively. Accordingly, we prepared a chromium-doped iron oxide with a chromium content of 8.4 mol% (corresponding to 8 wt% chromium) and an aluminium-doped iron oxide with an aluminium content of 8.4 mol%. Both catalysts contained 3 wt% Cu. The calcined catalyst precursors are referred to as M-HM or MCu-HM, where M is the metal dopant, and HM refers to hematite.

2.2. In situ Mössbauer spectroscopy

In situ Mössbauer spectra were recorded in an in-house reactor cell. A detailed description is provided elsewhere [25]. Gas flows were controlled with mass flow controllers. Water was added via a controlled evaporator mixer (Bronkhorst). In a typical experiment, the *in situ* Mössbauer spectroscopy cell was charged with 32.5 mg catalyst mixed with approximately 30 mg graphite. Experiments were performed at atmospheric pressure. After purging the cell in a He flow of 100 ml min^{-1} at room temperature for 3 min, the samples were exposed to reaction conditions at 450 °C in a gas flow with a steam to gas ratio of 0.5, containing steam (added as liquid water at a rate of 2.22 g $hour^{-1}$), H_2 (55 ml min^{-1}), CO (14 ml min^{-1}), and CO_2 (6 ml min^{-1}), while the He flow was reduced to 25 ml min^{-1}. Starting from this composition, the steam concentration was lowered in steps of 3 % until over-reduction was observed. After 1 hour at 450 °C, the temperature was lowered to 250 °C. At 250 °C, the H_2, CO, and CO_2 flows were replaced by He. After flushing for 3 min, water addition was stopped and the cell was allowed to cool to room temperature under a He flow. At room temperature, the gas inlet of the cell was closed, and a Mössbauer spectrum was recorded overnight. Most of the contribution of iron dissolved in the beryllium windows of the *in situ* Mössbauer cell was removed in the presented

Table 3
Fitting parameters of *in situ* Mössbauer spectra were obtained after exposure of the Cr-HM catalyst to gas mixtures of increased reducibility.

R	Phase	IS (mm s^{-1})	QS (mm s^{-1})	Hyperfine field (T)	Linewidth (mm s^{-1})	Spectral contribution (%)
1.48	Fe_3O_4(tet)	0.28	0.00	48.5	0.35	34
	Fe_3O_4(oct)	0.64	-0.03	44.0	0.37	66
1.64	Fe_3O_4(tet)	0.28	-0.01	48.6	0.34	33
	Fe_3O_4(oct)	0.64	-0.03	44.1	0.37	67
1.84	Fe_3O_4(tet)	0.28	0.00	48.4	0.37	33
	Fe_3O_4(oct)	0.65	-0.03	43.8	0.36	67
2.09	Fe_3O_4(tet)	0.28	-0.01	48.4	0.40	35
	Fe_3O_4(oct)	0.65	-0.02	44.1	0.38	65
2.42	Fe_3O_4(tet)	0.28	-0.01	48.4	0.35	34
	Fe_3O_4(oct)	0.64	-0.03	43.9	0.35	66
2.88	Fe_3O_4(tet)	0.28	-0.01	48.5	0.37	33
	Fe_3O_4(oct)	0.65	-0.03	44.0	0.38	67
4.60	Fe_3O_4(tet)	0.29	-0.01	48.4	0.34	33
	Fe_3O_4(oct)	0.65	-0.04	44.0	0.36	67
6.57	Fe_3O_4(tet)	0.28	-0.01	48.1	0.36	26
	Fe_3O_4(oct)	0.65	-0.02	43.7	0.34	52
	α-Fe	0.00	0.00	33.0	0.50	1
	Fe_3C	0.19	0.02	20.9	0.36	21

Experimental uncertainties: Isomer shift: IS ± 0.01 mm^{-1}, quadrupole splitting: QS ± 0.01 mm s^{-1}, line width: Γ ± 0.01 mm^{-1}, hyperfine magnetic field: ± 0.1 T, spectral contribution: ± 3 %.

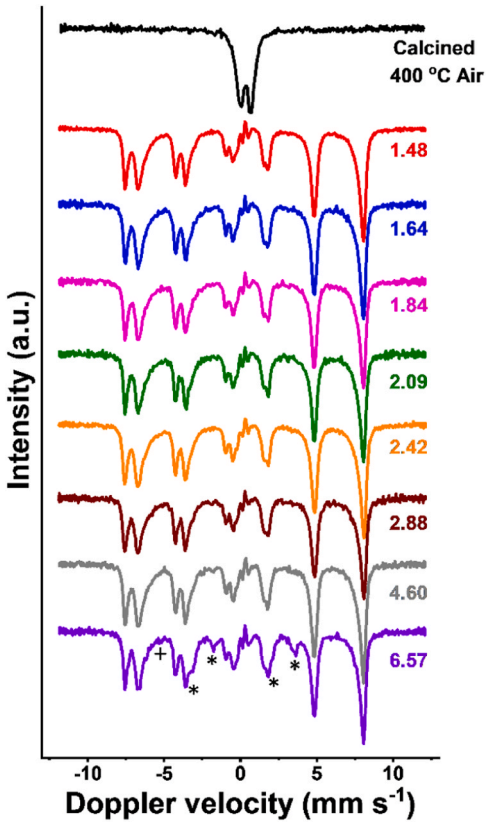

Fig. 3. *In situ* Mössbauer spectra of CrCu-HM catalyst compared to *ex situ* spectrum of calcined catalyst. Visible peaks of the cementite sextet are indicated with an asterisk (*), those of α-Fe with a plus (+).

spectra. In some spectra, minor features of the beryllium window remain at ~0.00 mm s^{-1}.

XRD patterns were recorded on a PANalitical X'pert pro diffractometer using a Cu-Kα source with a step size 0.008°. Spectral fitting was performed using HighScore Plus software. Catalysts discharged from the HTS reactors were exposed to air before XRD measurements.

3. Results and discussion

The detailed characterisation of the calcined catalyst precursors has been reported elsewhere [5,6,19]. An overview of the phases present in the calcined catalyst precursors is given in Table 1. In brief, XRD patterns and Mössbauer spectra show that the non-doped HM and chromium-doped Cr-HM reference samples consist of hematite. The other samples, *i.e.*, CrCu-HM, Al-HM, and AlCu-HM, contain a mixture of hematite and ferrihydrite. While XRD suggests the exclusive presence of hematite crystallites in all samples, room-temperature Mössbauer spectra indicate the presence of a Fe^{3+} superparamagnetic (SPM) phase. By recording Mössbauer spectra at −269 °C, it was shown that this Fe^{3+} SPM phase consisted of a mixture of ferrihydrite and hematite. The CrCu-HM, Al-HM, and AlCu-HM catalysts contain mainly ferrihydrite

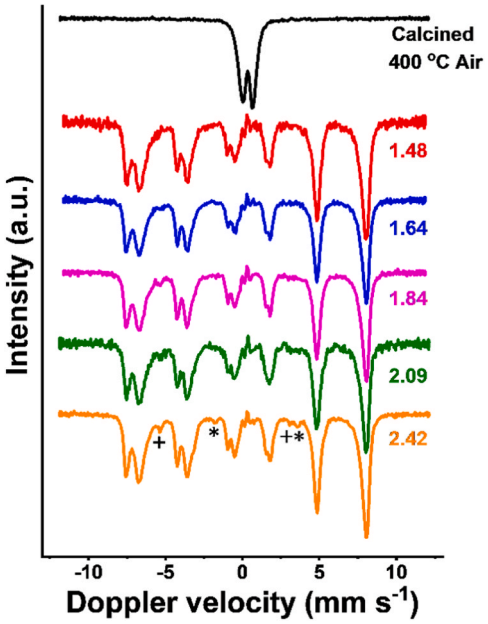

Fig. 4. *In situ* Mössbauer spectra of Al-HM catalyst compared to *ex situ* spectrum of calcined catalyst. Visible peaks of the cementite sextet are indicated with an (*), those of α-Fe with a (+).

Table 4
Fitting parameters of *in situ* Mössbauer spectra were obtained after exposure of the CrCu-HM catalyst to gas mixtures of increased reducibility.

R	Phase	IS (mm s^{-1})	QS (mm s^{-1})	Hyperfine field (T)	Linewidth (mm s^{-1})	Spectral contribution (%)
1.48	Fe_3O_4(tet)	0.28	-0.01	48.5	0.29	32
	Fe_3O_4(oct)	0.64	-0.03	44.2	0.36	68
1.64	Fe_3O_4(tet)	0.28	-0.01	48.5	0.31	33
	Fe_3O_4(oct)	0.65	-0.02	44.0	0.32	67
1.84	Fe_3O_4(tet)	0.28	0.00	48.5	0.3	33
	Fe_3O_4(oct)	0.64	-0.03	44.1	0.34	67
2.09	Fe_3O_4(tet)	0.28	-0.01	48.5	0.29	32
	Fe_3O_4(oct)	0.65	-0.03	44.0	0.34	68
2.42	Fe_3O_4(tet)	0.28	-0.01	48.7	0.32	33
	Fe_3O_4(oct)	0.65	-0.03	44.2	0.35	67
2.88	Fe_3O_4(tet)	0.28	-0.01	48.7	0.32	33
	Fe_3O_4(oct)	0.64	-0.03	44.2	0.32	63
	α-Fe	0.00	0.00	33.0	0.5	1
	Fe_3C	0.18	0.01	21.0	0.5	3
4.60	Fe_3O_4(tet)	0.29	0.00	48.5	0.32	33
	Fe_3O_4(oct)	0.64	-0.03	44.0	0.32	62
	α-Fe	0.00	0.00	33.0	0.5	1
	Fe_3C	0.17	0.09	20.4	0.5	4
6.57	Fe_3O_4(tet)	0.28	-0.01	48.5	0.3	28
	Fe_3O_4(oct)	0.65	-0.03	44.1	0.31	57
	Fe_3C	0.20	0.04	20.6	0.5	15

Experimental uncertainties: Isomer shift: IS ± 0.01 mm^{-1}, quadrupole splitting: QS ± 0.01 mm s^{-1}, line width: Γ ± 0.01 mm^{-1}, hyperfine magnetic field: ± 0.1 T, spectral contribution: ± 3 %.

Table 5
Fitting parameters of *in situ* Mössbauer spectra were obtained after exposure of the Al-HM catalyst to gas mixtures of increased reducibility.

R	Phase	IS (mm s^{-1})	QS (mm s^{-1})	Hyperfine field (T)	Linewidth (mm s^{-1})	Spectral contribution (%)
1.48	Fe_3O_4(tet)	0.29	-0.01	48.4	0.37	33
	Fe_3O_4(oct)	0.65	-0.03	44.5	0.35	67
1.64	Fe_3O_4(tet)	0.28	-0.02	48.4	0.37	36
	Fe_3O_4(oct)	0.65	-0.02	44.6	0.35	64
1.84	Fe_3O_4(tet)	0.28	-0.01	48.4	0.36	34
	Fe_3O_4(oct)	0.64	-0.03	44.7	0.33	62
	α-Fe	0.00	0.00	33.3	0.5	4
2.09	Fe_3O_4(tet)	0.28	-0.02	48.4	0.37	32
	Fe_3O_4(oct)	0.65	-0.02	44.7	0.35	61
	α-Fe	0.00	0.00	33.0	0.5	4
	Fe_3C	0.17	0.02	20.6	0.5	3
2.42	Fe_3O_4(tet)	0.28	-0.01	48.5	0.35	31
	Fe_3O_4(oct)	0.64	-0.03	44.7	0.34	59
	α-Fe	0.00	0.00	33.0	0.5	4
	Fe_3C	0.17	0.04	20.9	0.5	6

Experimental uncertainties: Isomer shift: IS ± 0.01 mm^{-1}, quadrupole splitting: QS ± 0.01 mm s^{-1}, line width: Γ ± 0.01 mm^{-1}, hyperfine magnetic field: ± 0.1 T, spectral contribution: ± 3 %.

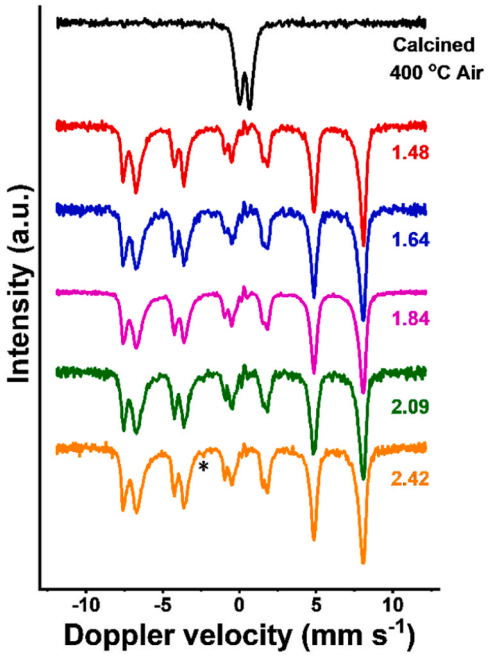

Fig. 5. *In situ* Mössbauer spectra of AlCu-HM catalyst compared to *ex situ* spectrum of calcined catalyst. Visible peaks of the cementite sextet are indicated with an (*).

with small contributions of hematite. On the contrary, the HM and Cr-HM reference catalysts only contain hematite.

We used *in situ* Mössbauer spectra to study the activation of the calcined HM precursor in a simulated HTS feed mixture as a function of the steam concentration. Table S1 lists the volumetric compositions investigated and the corresponding *R* ratios ($R = [CO]^*[H_2]/[CO_2]^*[H_2O]$) between the reducing gases H_2 and CO and the oxidizing gases H_2O and CO_2 [2]. The variations in the H_2O concentration were balanced by changing the He concentration to keep the CO, CO_2 and H_2 concentrations constant. The gas composition with the highest steam concentration of 27 % (*i.e.*, the lowest *R* of 1.48) is close to that of a commercial HTS feed with a steam to gas ratio of 0.5 (33 % steam) [4]. Starting from this composition, the steam concentration was lowered in steps of 3 % until over-reduction was observed.

Fig. 1 shows the *in situ* Mössbauer spectra of the used HM catalyst and the reference *ex situ* Mössbauer spectrum of the calcined precursor of HM. Exposure of the calcined HM catalyst to industrial HTS conditions with $R = 1.48$ results in the disappearance of the magnetically split sextet characteristic of hematite and the emergence of two new sextets related to the tetrahedral and octahedral Fe sites of magnetite (Table 2). No other Fe phases than magnetite were observed under these conditions. Increasing *R* to 1.64 and 1.84 (more reducing conditions) gave similar results. The onset of over-reduction was observed at $R = 2.09$ with the appearance of two more magnetically split sextets. The Mössbauer parameters of these sextets indicate the formation of α-Fe and Fe_3C (cementite) phases. At $R = 2.42$, the reduction is substantial, and the contribution of cementite is much larger than that of metallic Fe, indicating rapid carburisation of the latter. These samples did not contain wüstite (FeO), which is usually observed as an intermediate in the reduction of magnetite to metallic Fe during TPR experiments [21]. These results show that α-Fe and likely FeO are short-lived intermediates during the over-reduction of the active phase in HTS conditions to Fe-carbides under practical HTS conditions. These Fe-carbides are a significant cause of deactivation associated with over-reduction [1,9]. XRD patterns of the catalysts used in the *in situ* Mössbauer experiments are shown in Fig. S1. Consistent with the Mössbauer data, HM treated at $R = 1.48$ only contains magnetite. The same holds for the samples treated in the *R*-range of 1.64 – 2.42. However, unlike the Mössbauer findings, the catalysts exposed to $R = 2.09$ and 2.42 did not contain XRD evidence for the presence of cementite. A likely explanation is that the cementite phase is present as very small particles.

The corresponding Mössbauer spectra for Cr-HM are collected in Fig. 2. Similar to the non-doped HM catalyst, the hematite phase in the calcined chromium-doped catalyst precursor is completely converted into magnetite upon exposure to HTS conditions of $R = 1.48$ (Table 3). Unlike the HM catalyst, exposing Cr-HM to a feed with $R = 2.42$ does not lead to the formation of cementite. Thus, chromium doping renders the active magnetite phase more stable against over-reduction under industrially relevant HTS conditions. α-Fe and FeC_3 phases were only observed at $R = 6.57$ for this Cr-HM catalyst. These data show that chromium-doped magnetite is more stable against over-reduction, which aligns with literature [1,5]. The corresponding XRD patterns of the used Cr-HM catalysts confirm these findings (Fig. S2). However, in this case, XRD also showed the formation of cementite at $R = 6.57$.

The *in situ* Mössbauer spectra of the CrCu-HM catalyst are shown in Fig. 3. The reference spectrum of the calcined precursor contains an SPM doublet. Analysis of this sample by Mössbauer spectroscopy at −269 °C confirmed the presence of hematite and ferrihydrite (Table 1). After exposure of the calcined CrCu-HM catalyst to HTS conditions with $R = 1.48$, the SPM doublet disappeared, and two magnetically split sextets related to magnetite emerged (Table 4). At $R = 2.88$, an additional minor sextet appeared due to cementite. The fraction of cementite remained constant until $R = 4.60$. At $R = 6.57$ the contribution of the

Table 6
Fitting parameters of *in situ* Mössbauer spectra obtained after AlCu-HM catalyst exposure to increased reducibility gas mixtures.

R	Phase	IS (mm s^{-1})	QS (mm s^{-1})	Hyperfine field (T)	Linewidth (mm s^{-1})	Spectral contribution (%)
1.48	Fe_3O_4(tet)	0.28	-0.02	48.6	0.32	32
	Fe_3O_4(oct)	0.65	-0.02	44.8	0.32	68
1.64	Fe_3O_4(tet)	0.29	-0.03	48.5	0.35	34
	Fe_3O_4(oct)	0.65	-0.04	44.5	0.34	66
1.84	Fe_3O_4(tet)	0.29	-0.01	48.5	0.35	35
	Fe_3O_4(oct)	0.65	-0.03	44.7	0.33	65
2.09	Fe_3O_4(tet)	0.28	0.03	48.5	0.34	34
	Fe_3O_4(oct)	0.65	-0.03	44.7	0.33	64
	Fe_3C	0.18	0.09	20.5	0.50	2
2.42	Fe_3O_4(tet)	0.28	-0.01	48.5	0.34	33
	Fe_3O_4(oct)	0.65	-0.03	44.8	0.33	64
	α-Fe	0.00	0.00	33.0	0.50	1
	Fe_3C	0.18	0.00	21.0	0.50	2

Experimental uncertainties: Isomer shift: IS ± 0.01 mm^{-1}, quadrupole splitting: QS ± 0.01 mm s^{-1}, line width: Γ ± 0.01 mm^{-1}, hyperfine magnetic field: ± 0.1 T, spectral contribution: ± 3 %.

Table 7
Overview of phases observed *in situ* Mössbauer spectra.

	1.48	1.64	1.84	2.09	2.42	2.88	4.60	6.57
HM	●	●	●	●■♦	●♦	-	-	-
Cr-HM	●	●	●	●	●	●	●	●■♦
CrCu-HM	●	●	●	●	●	●■♦	●■♦	●♦
Al-HM	●	●	●■	●■♦	●■♦	-	-	-
AlCu-HM	●	●	●	●♦	●■♦	-	-	-

[a] Phases are indicated as: Magnetite (●), α-Fe (■), Fe_3C (♦).

cementite phase had grown much more significantly. Thus, the presence of copper leads to a slightly earlier onset of over-reduction in terms of *R*-value compared to Cr-HM. Nevertheless, the amount of over-reduced phases remains small, while the amount of cementite under the most reducing conditions for CrCu-HM was similar to that for Cr-HM. XRD patterns of the used CrCu-HM catalysts are shown in Fig. S3. The diffraction pattern after exposure of the calcined catalyst to HTS conditions of $R = 1.48$ shows that magnetite has been formed. No reflections due to phases obtained by over-reduction were observed between $R = 1.48$ and 2.42, which is in line with the *in situ* Mössbauer results. The discharged catalyst treated at $R = 2.88$ shows a weak diffraction line at $2\theta = \sim 45°$ in its XRD pattern, confirming the formation of a small amount of cementite in line with the *in situ* Mössbauer spectra (Fig. 3). This cementite feature was not observed for the discharged catalyst treated at $R = 4.60$, whereas it was visible in the XRD pattern of the catalyst treated at $R = 6.57$. The absence of cementite reflections in the used catalyst after exposure to HTS conditions with $R = 4.60$ confirms the utility of Mössbauer spectroscopy to investigate bulk iron species.

Exposure of the calcined Al-HM catalyst to HTS conditions of $R = 1.48$ resulted in the formation of the active magnetite phase, similar to the HM, Cr-HM, and CrCu-HM catalysts (Fig. 4). Upon exposure of the calcined catalyst to a gas mixture of $R = 1.64$, a third sextet was observed, which was attributed to α-Fe (Table 5), indicating over-reduction of the active magnetite phase. When the catalyst was subsequently exposed to more reducing conditions, the α-Fe phase was observed until a cementite phase formed at $R = 2.09$. This shows that the presence of aluminium in these catalysts enhances the over-reduction of the active phase to α-Fe, while it initially prevents carburization. The stabilisation of the α-Fe phase against carburization was not observed in the non-doped and chromium-doped catalysts. This could indicate that the α-Fe interacts with an amorphous Al_2O_3 phase invisible to XRD analysis, whose presence was hypothesized above. Despite the possible presence of a separate amorphous Al_2O_3 phase and the enhanced over-reduction caused by aluminium doping, the aluminium-doped catalyst was stable from over-reduction at a steam concentration of 27 % ($R = 1.48$), which is substantially lower than normal operating conditions where a steam concentration of 33 % is used [4]. This confirms the potential of aluminium to replace chromium as a dopant in Fe-based WGS catalysts [19]. The possible presence of a separate amorphous Al_2O_3 phase suggests that further optimisation of the preparation procedure should be explored to obtain an optimal ageing pH for aluminium and iron oxides. Natesakhawat et al. showed that the pH during precipitation significantly influenced the CO conversion of the catalysts. They suggested that this results from low pH values in the preparation, which would favour Fe precipitation, whereas precipitation of Al species is faster at high pH values. Although the authors mention that precipitated aluminium species can dissolve in water at pH > 9, it is also mentioned in other works that the optimum pH is 11. XRD patterns of the used Al-HM catalysts (Fig. S4) confirm the formation of magnetite upon exposure of the calcined catalyst to HTS conditions at $R = 1.48$. No reflections belonging to α-Fe were observed at $R = 1.64$–2.09, in contrast to the *in situ* Mössbauer spectra where α-Fe formation was observed at $R = 1.64$ and below. Since these patterns were recorded after the catalysts were exposed to air, the α-Fe phase observed in the Mössbauer spectra is likely oxidised. This shows the benefit of using *in situ* Mössbauer spectroscopy. No evidence of a separate aluminium oxide phase was found, consistent with the presence of an amorphous aluminium oxide phase.

In situ Mössbauer spectra of AlCu-HM catalysts (Fig. 5, Table 6) show α-Fe and cementite formation at $R = 2.09$. As this is similar to the non-doped HM catalyst, it can be stated that these dopants do not affect

catalyst over-reduction. It should be mentioned that the steam content corresponding to $R = 2.09$, 18 %, is far below the normal operating conditions of 33 % steam typically employed in an industrial plant. This means that the AlCu-HM catalyst is a viable candidate for replacing chromium. Notably, the effect of aluminium/copper co-doping is opposite to that of chromium/copper co-doping, where a slight enhancement of over-reduction was found. The stabilization of α-Fe, observed in the aluminium-doped catalyst, was not observed in the aluminium/copper co-doped catalyst. Since our study did not optimise the preparation procedure for the aluminium-doped catalysts, we cannot exclude the presence of a separate amorphous Al_2O_3 phase. Based on these results, further optimization of the aluminium precipitation procedure should be explored. XRD patterns of used AlCu-HM catalysts confirm the formation of the active magnetite catalysts at $R = 1.48$ (Fig. S5). In contrast to the *in situ* Mössbauer spectra, no reflections due to cementite were observed in the sample treated at $R = 2.42$, suggesting that, if present, it is in the form of very small particles.

4. Conclusions

The influence of chromium and aluminium doping and copper co-doping of iron oxide based HTS catalysts was investigated for the first time with *in situ* Mössbauer spectroscopy (Table 7). *In situ* Mössbauer spectra showed that in a non-doped iron-oxide catalyst, α-Fe and cementite formation occurred after treatment under HTS conditions at an R factor of 2.09. Doping with chromium stabilized the active magnetite phase down to $R = 4.60$ before α-Fe and cementite formation occurred. The chromium-copper co-doped catalyst slightly enhanced the over-reduction of the active magnetite phase to an R factor of 2.88. In contrast, the aluminium-doped catalysts only showed α-Fe formation at $R = 1.64$. Cementite formation was observed at $R = 2.09$ for the aluminium-doped catalyst, which shows that the α-Fe is stabilized from carburization in aluminium-doped catalysts. Cementite formation was observed at R = 2.09 in the aluminium-copper co-doped catalyst, the same as for a non-doped catalyst. Despite the enhanced over-reduction in the aluminium-doped catalyst compared to the chromium-doped catalyst, no over-reduction was observed at $R = 1.48$, corresponding to a steam concentration of 27 %. This steam concentration is significantly lower than industrial operating conditions of 33 % H_2O. Optimisation of the precipitation pH is necessary to ensure optimal incorporation of the aluminium dopant in the catalyst.

CRediT authorship contribution statement

Achim Iulian Dugulan: Writing – review & editing, Supervision, Resources, Methodology. **Leon van de Water**: Writing – review & editing, Validation, Supervision, Methodology, Funding acquisition, Conceptualization. **Emiel Hensen**: Writing – review & editing, Validation, Funding acquisition, Conceptualization. **Maxim Ismaële Ariëns**: Writing – original draft, Investigation, Formal analysis. **Ekkes Brück**: Writing – review & editing, Validation, Resources, Project administration.

Declaration of Competing Interest

The authors declare that they have no known competing financial interests or personal relationships that could have appeared to influence the work reported in this paper.

Data Availability

Data will be made available on request.

Appendix A. Supporting information

Supplementary data associated with this article can be found in the online version at doi:10.1016/j.apcatb.2024.124316.

References

[1] Minghui Zhu, Israel E. Wachs, Iron-based catalysts for the high-temperature water-gas shift (HT-WGS) reaction: a review, ACS Catal. *6* (2016) 722–732.
[2] Myung Suk Lee Dae-Won Lee, Joon Yeob Lee, Seongmin, Hee-Jun Eom Kim, Ju. Moon Dong, Lee Kwan-Young, The review of Cr-free Fe-based catalysts for high-temperature water-gas shift reactions, Catal. Today *210* (2013) 2–9.
[3] David S. Newsome, The water-gas shift reaction, Catal. Rev. Sci. Eng. *21* (1980) 275–318.
[4] Martyn V..Twigg Catalyst handbook; 2 ed.; 1989.
[5] M.I. Ariëns, V. Chlan, P. Novák, L.G.A. van de Water, A.I. Dugulan, E. Brück, E.J. M. Hensen, The role of chromium in iron-based high-temperature water-gas shift catalysts under industrial conditions, Appl. Catal. B: Environ. *297* (2021) 120465.
[6] L.G.A. M.I.Ariëns, A.I. van de Water, E. Dugulan, E.J.M.Hensen Brück, Copper promotion of chromium-doped iron oxide water-gas shift catalysts under industrially relevant conditions, J. Catal. *405* (2021) 391–403.
[7] J. Christopher, Minghui Zhu Keturakis, K. Emma, Marco Daturi Gibson, Anatoly Franklin Tao, I. Frenkel, E.Wachs Israel, Dynamics of CrO_3-Fe_2O_3 catalysts during the high-temperature water-gas shift reaction: molecular structures and reactivity, ACS Catal. *6* (2016) 4786–4798.
[8] Tulio C.R.Rocha Minghui Zhu, Axel Knop-Gericke Thomas Lunkenbein, Israel E. Wachs Robert Schlogl, Promotion mechanisms of iron oxide-based high temperature water-gas shift catalysts by chromium and copper, ACS Catal. *6* (2016) 4455–4464.
[9] C. Rhodes, G.J. Hutchings, A.M. Ward, Water-gas shift reaction: finding the mechanistic boundary, Catal. Today *23* (1995) 43–58.
[10] Pengfei Tian Minghui Zhu, Michael Jiacheng Chen, E. Ford, Israel E.Wachs Jing Xu, Yi-Fan Han, Activation and deactivation of the commercial-type CuO-Cr_2O_3-Fe_2O_3 high temperature shift catalyst, Am. Inst. Chem. Eng. *66* (2019) 1–6.
[11] Pengfei Tian Minghui Zhu, Thomas Lunkenbein Ravi Kurtz, Robert Schlogl Jing Xu, Yi-Fan Han Israel E.Wachs, Strong metal–support interactions between copper and iron oxide during the high-temperature water-gas shift reaction, Angew. Chem. *131* (2019) 9181–9185.
[12] C. Pellerin, S.M. Booker, Reflections on hexavalent chromium: health hazards of an industrial heavyweight, Environ. Health Perspect. *108* (2000) 402–407.
[13] Minghui Zhu, Özgen Yalçin, Israel E. Wachs, Revealing structure-activity relationships in chromium free high temperature shift catalysts promoted by earth abundant elements, Appl. Catal. B Environ. *232* (2018) 205–212.
[14] K. Gunugunuri, Reddy, P. Kapila Gunasekara, Boolchand, G. Panagiotis, Smirniotis Cr- and Ce-doped ferrite catalysts for the high temperature water-gas shift reaction: TPR and Mössbauer spectroscopic study, J. Phys. Chem. C. *115* (2011) 920–930.
[15] Devaiah Damma, Deshetti Jampaiah, Aaron Welton, Punit Boolchand, Antonios Arvanitis, Junhang Dong, Panagiotis G. Smirniotis, Effect of Nb modification on the structural and catalytic property of Fe/Nb/M (M = Mn, Co, Ni, and Cu) catalyst for high temperature water-gas shift reaction, Catal. Today *355* (2019) 921–931.
[16] Minghui Zhu, Israel E. Wachs, A perspective on chromium-Free iron oxide-based catalysts for high temperature water-gas shift reaction, Catal. Today *311* (2018) 2–7.
[17] Sittichai Natesakhawat, Xueqin Wang, Lingzhi Zhang, Umit S. Ozkan, Development of chromium-free iron-based catalysts for high-temperature water-gas shift reaction, J. Mol. Catal. A Chem. *260* (2006) 82–94.
[18] Fereshteh Meshkani, Mehran Rezaei, Preparation of nanocrystalline metal (Cr, Al, Mn, Ce, Ni, Co and Cu) modified ferrite catalysts for the high temperature water gas shift reaction, Renew. Energy *74* (2015) 588–589.
[19] M.I. Ariëns, L.G.A. van de Water, A.I. Dugulan, E. Brück, E.J.M. Hensen, Substituting chromium in iron-based catalysts for the high-temperature water-gas shift reaction, ACS Catal. 12 (22) (2022) 13838–13852.
[20] Genira Carneiro de Araújo, Maria do Carmo Rangel, An environmental friendly dopant for the high-temperature shift catalysts, Catal. Today *62* (2000) 201–207.
[21] Dae-Woon Jeong, Jae-Oh Vijayanand Subramanian, Won-Jun Shim, Yong-Chil Jang, Hyun-Seog Seo, Roh; Jae Hoi Gu; Yong Taek Lim High-temperature water gas shift reaction over Fe/Al/Cu oxide based catalysts using simulated waste-derived synthesis gas, Catal. Lett. *143* (2013) 438–444.
[22] W.K. Jozwiak, E. Kaczmarek, T.P. Maniecki, W. Ignaczak, W. Maniukiewicz, Reduction behavior of iron oxides in hydrogen and carbon monoxide atmospheres, Appl. Catal. A Gen. *326* (2007) 17–27.
[23] P.Santos Vera, A.Wezendonk Tim, A. Juan José Delgado Jaén, Iulian Dugulan, Maxim A. Nasalevich, Adam Chojecki Husn-Ubayda Islam, Xiaohui Sun Sina Sartipi, Abrar A. Hakeem, Ard C.J. Koeken, Thomas Davidian Matthijs Ruitenbeek, R. Garry, Meima Gopinathan Sankar, Michiel Makkee Freek Kapteijn, Jorge Gascon, Metal organic framework-mediated synthesis of highly active and stable Fischer-Tropsch catalysts, Nat. Commun. *6* (2015) 6451.
[24] Hirsa Jingxiu Xie, M. Torres Galvis, C.J. Ard, Alexey Kirilin Koeken, Matthijs Ruitenbeek A.Iulian Dugulan, P. de Jong Krijn, Size and promoter effects on stability of carbon-nanofiber-supported iron-based Fischer-Tropsch catalysts, ACS Catal. *6* (2016) 4017–4024.
[25] A. Tim, Vera Wezendonk, P. Santos, A. Maxim, Quirinus Nasalevich, S.E. Warringa, A. Iulian Dugulan, Ard Adam Chojecki, C.J. Koeken, Garry Meima Matthijs Ruitenbeek, Gopinathan Sankar Husn-Ubayda Islam, Freek Kapteijn Michiel Makkee, Jorge Gascon, Elucidating the nature of fe species during pyrolysis of the Fe-BTC MOF into highly active and stable Fischer–Tropsch catalysts, ACS Catal. *6* (2016) 3236–3247.